ACS APPLIED NANO MATERIALS

www.acsanm.org

Article

Zinc Gallate Nanoplates on Microporous Organic Hollow Nanoplatforms for Enhanced Reductive CO_2 Fixation to Formamides

Hyun Su Kim, June Young Jang, Yoon-Joo Ko, Hye-Young Jang, and Seung Uk Son*

Cite This: *ACS Appl. Nano Mater.* 2024, 7, 12752−12760

Read Online

ACCESS | Metrics & More | Article Recommendations | Supporting Information

ABSTRACT: This work suggests an engineering methodology for catalytic 2D materials to achieve more efficient catalytic systems. Zinc gallate (ZnG), a Lewis acidic material with a thin 2D morphology, can easily form aggregates through layer−layer packing. Inner parts of ZnG aggregates would have difficulty in interacting with substrates. By coating hollow microporous organic polymer (H-MOP) supports with ZnG, the catalytic performance of ZnG can be enhanced due to facilitated contact of substrates with Zn species in shells. H-MOP@ZnG-2 with an optimal ZnG coating showed a much enhanced catalytic performance for the reductive carbon dioxide fixation with amines to formamides compared with ZnG. Various amines can be utilized in the reductive carbon dioxide fixation to formamides. In addition, H-MOP@ZnG-2 showed recyclability, maintaining its catalytic performance for five successive reactions.

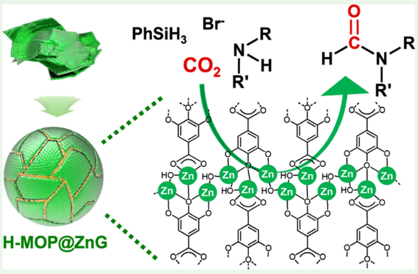

KEYWORDS: *nanocatalyst, zinc, carbon dioxide, hollow material, nanoplate, microporous organic polymer*

■ INTRODUCTION

As climate change poses a growing threat to humanity, the need to decrease greenhouse gas emissions becomes ever more critical.[1,2] Carbon dioxide emission is an unavoidable consequence of the use of petroleum as an energy source. Thus, the significance of capturing and utilizing carbon dioxide cannot be overstated. An efficient fixation of carbon dioxide into chemicals is an effective method for reducing carbon dioxide in the atmosphere.[3] Moreover, to achieve more efficient conversions, the development of efficient catalysts is necessary.[4−6]

Recently, the reductive carbon dioxide fixation to formamides has attracted significant attention from scientists due to its mild reaction conditions.[7−10] The reaction of carbon dioxide with amines in the presence of silanes can induce the formation of formamides. Efficient Lewis acid catalysts enable this conversion to take place even at room temperature.[11−30]

Recently, zinc-based Lewis acid catalysts have been studied for various carbon dioxide conversions to valuable chemicals due to the abundance, relatively lower toxicity, and colorless nature of a zinc element.[31−38] For example, zinc phenoxides have been reported to catalyze a carbon dioxide conversion with epoxides to polycarbonates.[32,33] However, due to their homogeneous catalytic feature, they have limitations in their utilization in industrial processes. In this regard, over the past decade, heterogeneous Zn-based Lewis acid catalysts have been developed.[34−38] As a representative example, insoluble zinc glutarate (ZnGA) has been developed through a reaction of zinc precursors with glutaric acids.[39,40] Furthermore, it has been applied as an industrial catalyst for the synthesis of polycarbonates via a carbon dioxide conversion with epoxides.[39,40] While ZnGA has shown promising selectivity in the insertion of carbon dioxide into polymer chains of polycarbonates, its low catalytic activity (<0.5 kg polycarbonate/cat g) remains a critical drawback.

There have been numerous efforts to find better ligands to replace the glutaric acid of ZnGA.[41] However, resultant Zn-based materials could not surpass the catalytic activity of ZnGA. Recently, our research group has discovered that zinc gallate (ZnG) having a thin morphology surpasses the catalytic activity of ZnGA, while maintaining the selectivity in the insertion of carbon dioxide.[42] However, ZnG has two important drawbacks. First, although surfaces of 2D ZnG plates are highly active for carbon dioxide conversion, they can be easily packed to form aggregates (Figure 1), resulting in decreased catalytic activity. Second, the recovery and recycling of ZnG are technically difficult due to its thin feature.

It can be speculated that thin ZnG can be loaded onto solid supports not only to induce efficient utilization of surfaces but also to facilitate easy separation from reaction mixtures. Especially, if hollow nanosupports are employed, the engineering of hollow-structured heterogeneous catalysts can be achieved. It is noteworthy that recently hollow nanocatalysts have been reviewed as advanced heterogeneous catalytic

Received: March 3, 2024
Revised: April 24, 2024
Accepted: May 6, 2024
Published: May 18, 2024

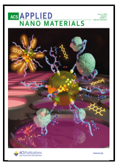

https://doi.org/10.1021/acsanm.4c01287
ACS Appl. Nano Mater. 2024, 7, 12752−12760

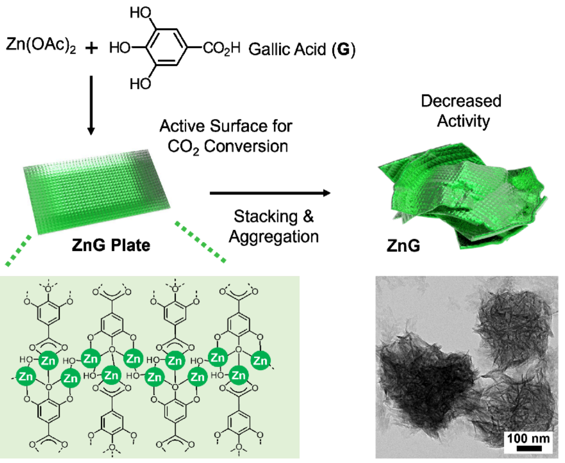

Figure 1. Formation of thin zinc gallate (ZnG) and TEM image showing conventional aggregates of ZnG.

systems, thanks to the facilitated mass transfer of substrates and the efficient utilization of catalytic sites.[43]

Recently, microporous organic polymers (MOPs) have emerged as new platforms for functional materials.[44] MOPs are prepared through networking of organic building blocks.[44] Our research group has reported the engineering of hollow MOPs (H-MOPs) using silica nanospheres as templates.[45] Because shells of H-MOPs have a microporosity, precursors of secondary functional materials can be easily loaded on MOP networks. In this regard, H-MOPs can be utilized as platforms for engineering hollow nanomaterials. Particularly, ZnG can be engineered on H-MOPs to form hollow H-MOP@ZnG materials, realizing efficient heterogeneous catalytic systems. In this work, we report the engineering of H-MOP@ZnG using H-MOPs as platforms and their enhanced catalytic performance in the reductive fixation of carbon dioxide to formamides at room temperature.

■ EXPERIMENTAL SECTION

General Information. Morphologies and chemical distributions of the materials were investigated by transmission electron microscopy (TEM) using a JEM2100F microscope. Surface areas and porosity of materials were characterized through analysis of N_2 and CO_2 adsorption−desorption isotherm curves obtained using a Micromeritics ASAP2020 instrument. Pore size distributions of materials were obtained through the analysis of N_2 adsorption−desorption isotherm curves based on the nonlocal density functional theory (NLDFT) method. Powder X-ray diffraction (PXRD) patterns were obtained using a Rigaku MAX-2200 instrument. Zinc contents of materials were characterized by inductively coupled plasma atomic emission spectroscopy (ICP-AES) using an OPTIMA 8300 analyzer. Infrared absorption (IR) spectroscopy was conducted using a Bruker VERTEX70 spectrometer. X-ray photoelectron spectroscopy (XPS) was conducted using a Thermo VG spectrometer. Solid-state ^{13}C nuclear magnetic resonance spectroscopy was conducted in cross-polarization (CP)/total sideband suppression (TOSS) mode using a 500 MHz Bruker ADVANCE II NMR spectrometer. Solution-state ^{1}H and ^{13}C NMR spectra were obtained by using a Bruker Ascend 500 spectrometer at the Chiral Material Core Facility Center of Sungkyunkwan University. Thermogravimetric analysis (TGA) was conducted using a TG/DTA7300 instrument.

Synthesis of H-MOP@ZnGs and ZnG. For the preparation of H-MOP, silica nanospheres were prepared by the Stöber method reported in the literature.[46] In this work, the following procedures were applied to the preparation of silica templates. Ethanol (200 mL), water (8 mL), and ammonia solution (28−30%, 5 mL) were added to a 250 mL round-bottomed flask. After the mixture was stirred at room temperature for 1 h, tetraethyl orthosilicate (14 mL) was added. After the mixture was stirred for 18 h at room temperature, a mixture of hexane (400 mL) and methylene chloride (50 mL) was added. Silica spheres were separated by centrifugation, washed with a mixture of methanol (20 mL) and acetone (20 mL) three times, and dried under a vacuum.

Silica nanospheres (0.50 g), $(PPh_3)_2PdCl_2$ (14 mg, 20 μmol), CuI (3.8 mg, 20 μmol), triethylamine (40 mL), and distilled toluene (10 mL) were added to a flame-dried 100 mL Schlenk flask under argon. After the reaction mixture was sonicated for 1 h at room temperature, tetra(4-ethynylphenyl)methane (83 mg, 0.20 mmol) and 1,4-diiodobenzene (0.13 g, 0.40 mmol) dissolved in toluene (10 mL) were added. After being stirred at 90 °C for 24 h, the reaction mixture was cooled to room temperature. SiO_2@MOP was separated by centrifugation, washed with a mixture of acetone (20 mL), methylene chloride (10 mL), and methanol (10 mL) five times, and dried under vacuum. SiO_2@MOP was added to a mixture of an aqueous HF solution (48%, 7.5 mL), water (7.5 mL), and methanol (25 mL) in a 50 mL Falcon tube. *Caution: HF solution is extremely toxic and should be handled with specific gloves in a hood.* After stirring for 6 h at room temperature, solids (H-MOPs) were separated by centrifugation, washed with a mixture of water (10 mL) and methanol (30 mL) five times, and dried under vacuum.

For preparation of H-MOP@ZnG-2, H-MOP (25 mg) was dispersed in distilled methanol (6.5 mL) in a flame-dried 50 mL Schlenk flask under argon. After the sample was sonicated for 1 h at room temperature, zinc acetate dihydrate (76 mg, 0.35 mmol) and gallic acid monohydrate (65 mg, 0.35 mmol) dissolved in distilled methanol (10 mL) were added. After being stirred at 50 °C for 48 h, the reaction mixture was cooled to room temperature. Solids (H-MOP@ZnG-2) were separated by centrifugation, washed with distilled methanol (40 mL) five times, and dried under a vacuum. For preparation of H-MOP@ZnG-1, the same synthetic procedures as H-MOP@ZnG-2 were applied, except that zinc acetate dihydrate (25 mg, 0.12 mmol) and gallic acid monohydrate (22 mg, 0.12 mmol) dissolved in distilled methanol (10 mL) were used. For the preparation of H-MOP@ZnG-3, the same synthetic procedures as H-MOP@ZnG-2 were applied except using zinc acetate dihydrate (0.13 g, 0.58 mmol) and gallic acid monohydrate (0.11 g, 0.58 mmol) dissolved in distilled methanol (10 mL). The control material ZnG was prepared by the same synthetic procedures as H-MOP@ZnG-2 without using H-MOP.

Procedures of Catalytic Studies. For the reductive carbon dioxide conversion to formamides, H-MOP@ZnG-2 (4.4 mg, 1.0 mol % Zn to amines), amine (1.0 mmol), phenylsilane ($PhSiH_3$, 0.25 mL, 2.0 mmol), tetrabutylammonium bromide (TBAB, 3.2 mg, 1.0 mol % to amines), and distilled acetonitrile (3 mL) were added to an autoclave. Based on these representative conditions, various reaction conditions, such as the amount of reagents, were applied. After the autoclave was closed, carbon dioxide flew through the valves. After the autoclave was charged with carbon dioxide (10 bar), the reaction mixture was stirred for 12 h at room temperature. After carbon dioxide was released, the reaction mixture was transferred to a flask by using chloroform. After the H-MOP@ZnG catalysts were recovered from a reaction mixture through centrifugation, volatile solvents were evaporated. The residues in the flask were analyzed by ^{1}H and ^{13}C NMR studies (Figure S1). Products were isolated by flash column chromatography. For recyclability tests, after catalytic reaction, H-MOP@ZnG-2 was recovered through centrifugation, washed with ethyl acetate and acetone, dried under a vacuum, and used for the next run. Formamide products (**P1** to **P6**) were known compounds, and their NMR spectra matched those in the literature.[16,38,47,48]

Characterization Data of Amides. **P1**[38] with a rotamer ratio of 95:5 and an isolated yield of 97%. ^{1}H NMR (500 MHz, $CDCl_3$) δ = 8.48 (s, 0.95H), 8.37 (s, 0.05H), 7.42 (t, J = 7.9 Hz, 2H), 7.28 (t, J = 7.4 Hz, 1H), 7.18 (d, J = 7.4 Hz, 2H), 3.36 (s, 0.15H), 3.33 (s, 2.85H) ppm. ^{13}C NMR (125 MHz, $CDCl_3$) δ = 162.4, 142.2, 129.6, 126.4, 122.4, 32.1 ppm. HRMS (EI): m/z calcd for $C_8H_{10}NO$ $[M + H]^+$ 136.0762; found: 136.0758. **P2**[38] with a rotamer ratio of 50:50

and an isolated yield of 96%. ^{1}H NMR (500 MHz, $CDCl_3$) δ = 8.69 (d, J = 11.4 Hz, 0.5H), 8.39 (d, J = 1.1 Hz, 0.5H), 7.54 (m, 1H), 7.35 (m, 2H), 7.15 (m, 2H) ppm. ^{13}C NMR (125 MHz, $CDCl_3$) δ = 162.7, 159.1, 136.9, 136.7, 129.8, 129.1, 125.3, 124.9, 120.0, 118.9 ppm. HRMS (EI): m/z calcd for C_7H_8NO $[M + H]^+$ 122.0606; found: 122.0602. **P3**[16,38] with a rotamer ratio of 86:14 and an isolated yield of 95%. ^{1}H NMR (500 MHz, $CDCl_3$) δ = 8.28 (s, 0.86H), 8.22 (d, J = 11.9 Hz, 0.14H), 7.33 (m, 5H), 5.77 (br, 1H), 4.51 (d, J = 5.9 Hz, 1.71H), 4.44 (d, J = 6.5 Hz, 0.29H) ppm. ^{13}C NMR (125 MHz, $CDCl_3$) δ = 164.7, 161.1, 137.6, 137.5, 129.0, 128.8, 128.0, 127.8, 127.7, 127.0, 45.7, 42.2 ppm. HRMS (EI): m/z calcd for $C_{11}H_{16}NO$ $[M + H]^+$ 178.1232; found: 178.1231. **P4**[47,48] with a rotamer ratio of 77:23 and an isolated yield of 94%. ^{1}H NMR (500 MHz, $CDCl_3$) δ = 8.14 (s, 0.23H), 8.10 (s, 0.77H), 5.53 (br s, 0.23H), 5.39 (br s, 0.77H), 3.88 (m, 0.77H), 3.32 (m, 0.23H), 1.92 (m, 2H), 1.70 (m, 3H), 1.27 (m, 5H) ppm. ^{13}C NMR (125 MHz, $CDCl_3$) δ = 163.6, 160.3, 51.0, 47.1, 34.7, 33.1, 25.4, 25.0, 24.7 ppm. HRMS (EI): m/z calcd for $C_7H_{14}NO$ $[M + H]^+$ 128.1075; found: 128.1070. **P5**,[38] an isolated yield of 93%. ^{1}H NMR (500 MHz, $CDCl_3$) δ = 8.06 (s, 1H), 3.70 (t, J = 4.8 Hz, 2H), 3.67 (t, J = 4.8 Hz, 2H), 3.58 (t, J = 4.8 Hz, 2H), 3.40 (t, J = 4.8 Hz, 2H) ppm. ^{13}C NMR (125 MHz, $CDCl_3$) δ = 160.9, 67.2, 66.5, 45.8, 40.6 ppm. HRMS (EI): m/z calcd for $C_5H_{10}NO_2$ $[M + H]^+$ 116.0712; found: 116.0705. **P6**,[47] an isolated yield of 94%. ^{1}H NMR (500 MHz, $CDCl_3$) δ = 8.03 (s, 1H), 3.58 (m, 2H), 3.40 (m, 2H), 2.40 (m, 4H), 2.32 (s, 3H) ppm. ^{13}C NMR (125 MHz, $CDCl_3$) δ = 160.8, 55.4, 54.2, 46.1, 45.6, 39.9 ppm. HRMS (EI): m/z calcd for $C_{10}H_{12}NO$ $[M + H]^+$ 162.0919; found: 162.0912.

■ RESULTS AND DISCUSSION

Figure 2 reveals synthetic schemes of H-MOP and H-MOP@ZnGs (refer to the Experimental Section for detailed synthetic procedures). First, using silica spheres as templates, H-MOPs were prepared through the Sonogashira coupling of tetra(4-ethynylphenyl)methane with 2 equiv of 1,4-diiodobenzene, followed by silica etching.[49] In the presence of H-MOPs, ZnG was formed through a reaction of zinc acetate dihydrate with 1 equiv of gallic acid to generate H-MOP@ZnGs. With a fixed amount of H-MOP (25 mg), amounts of zinc acetate dihydrate and gallic acid gradually increased from 0.12 mmol to 0.35 and 0.58 mmol, and the corresponding materials were denoted as H-MOP@ZnG-1, H-MOP@ZnG-2, and H-MOP-ZnG-3, respectively.

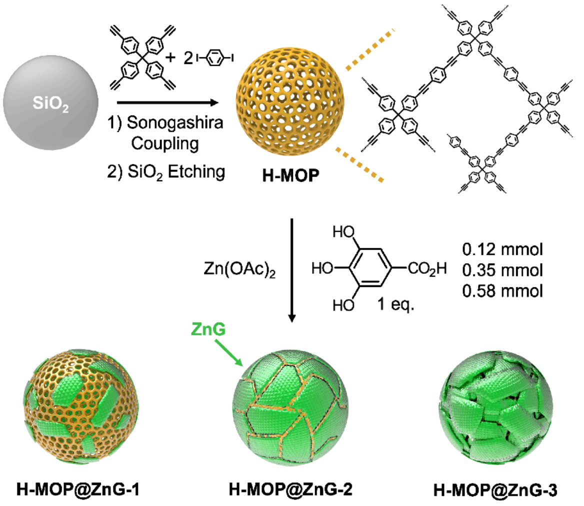

Figure 2. Synthetic schemes of H-MOP and H-MOP@ZnGs.

Morphologies of materials were investigated by TEM analysis (Figure 3 and Figure S2). H-MOP platforms showed a hollow structure with an average diameter of 200 nm and an average shell thickness of 16 nm (Figure S2). As ZnG was introduced to H-MOP, the shell thicknesses of H-MOP@ZnGs gradually increased from 19 nm (H-MOP@ZnG-1) to 24 nm (H-MOP@ZnG-2) and 30 nm (H-MOP@ZnG-3) (Figures 3a–i and 4a).

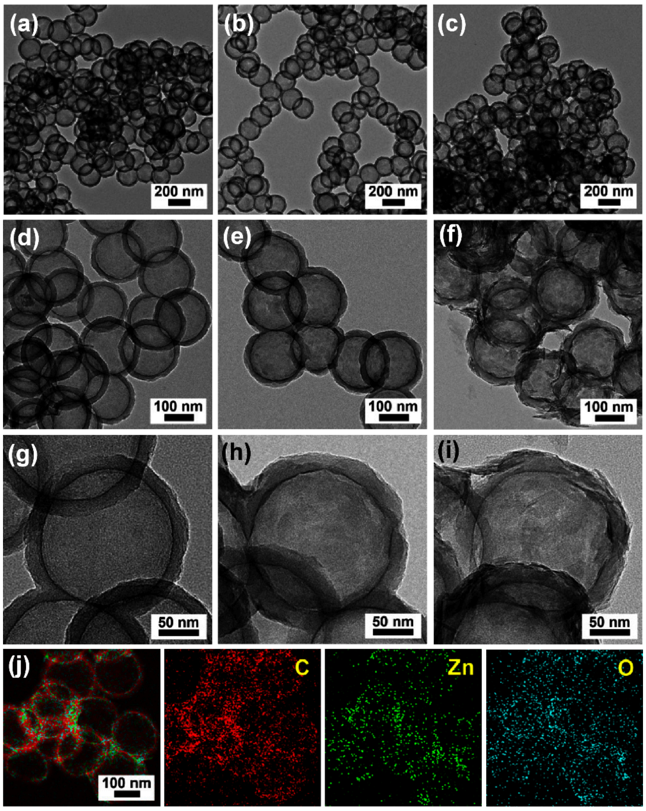

Figure 3. TEM images of (a, d, g) H-MOP@ZnG-1, (b, e, h) H-MOP@ZnG-2, and (c, f, i) H-MOP@ZnG-3. (j) EDS-based elemental mapping images of H-MOP@ZnG-2.

Corresponding diameters of H-MOP@ZnG-1, H-MOP@ZnG-2, and H-MOP@ZnG-3 were measured to be 208, 222, and 230 nm, respectively, indicating that ZnG was successfully incorporated into shells of H-MOP@ZnGs with increased amounts of ZnG. In the case of H-MOP@ZnG-3, independent ZnG plates were additionally observed, indicating that ZnGs exceeded the optimal amount for uniform loading on H-MOP platforms. While the shells of H-MOPs had smooth surfaces (Figure S2), those of H-MOP@ZnGs were bumpy (Figure 3d–i). As amounts of ZnG increased, shell surfaces of H-MOP@ZnGs became bumpier, indicating that ZnG was incorporated into the shells of materials. In comparison, ZnG materials obtained without using H-MOP platforms showed irregular aggregates with a broad size distribution in the range of 100–500 nm (Figure 1).

Through ICP-AES studies on materials, contents of Zn in H-MOP@ZnG-1, H-MOP@ZnG-2, H-MOP@ZnG-3, and ZnG were analyzed to be 6.9, 14.9, 20.2, and 34.0 wt %, respectively (Figure 4b).

To analyze surface areas and porosity of materials, N_2 adsorption–desorption isotherm curves were obtained at 77 K. Analysis of the isotherm curves of H-MOP based on the Brunauer–Emmett–Teller (BET) theory revealed a high surface area of 683 m^2/g and microporosity (pore sizes <2 nm) with a micropore volume of 0.15 cm^3/g (Figure 4c,d and Table S1). As the amount of ZnG increased, surface areas of

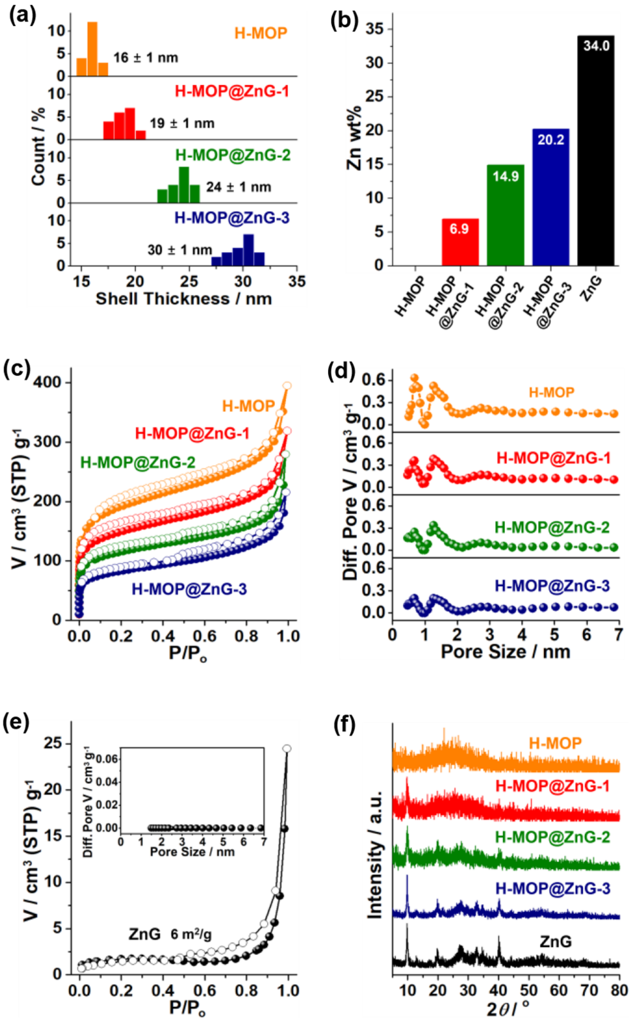

Figure 4. (a) Shell thickness distribution diagrams. (b) Zn contents analyzed by ICP-AES. (c, e) N_2 adsorption−desorption isotherm curves obtained at 77 K. (d, inset of e) Pore size distribution diagrams obtained by the NLDFT method. (f) PXRD patterns of H-MOP, H-MOP@ZnGs, and ZnG.

H-MOP@ZnG gradually decreased from 537 m^2/g (H-MOP@ZnG-1) to 423 m^2/g (H-MOP@ZnG-2) and 302 m^2/g (H-MOP@ZnG-3) (Figure 4c). Accordingly, the micropore volumes of H-MOP@ZnGs gradually decreased from 0.12 cm^3/g (H-MOP@ZnG-1) to 0.091 cm^3/g (H-MOP@ZnG-2) and 0.054 cm^3/g (H-MOP@ZnG-3) (Figure 4d). In comparison, ZnG powder showed a relatively low surface area of 6 m^2/g without microporosity (Figure 4e and inset). These observations rationalize the decreased surface areas of H-MOP@ZnGs, compared with that of H-MOP, and the successful loading of ZnG on the H-MOP platforms.

Powder XRD studies revealed that the ZnG is a crystalline material with main diffraction peaks at 2θ values of 9.8°, 20.0°, 27.6°, 32.7°, 34.7°, and 40.2°, corresponding to (100), (102/200), (221/130/212), (232/230), (004/302), and (330/204/400) crystalline planes of the ZnG reported in the literature (Figure 4f).[42] In comparison, H-MOP was amorphous, matching with conventional features of MOPs reported in the literature.[44] Thus, as the amounts of ZnG in H-MOP@ZnGs increased, diffraction peaks of ZnG gradually increased in their intensities and became sharper.

Chemical components of H-MOP@ZnGs were further characterized by IR, XPS, and solid-state ^{13}C NMR studies (Figure 5).

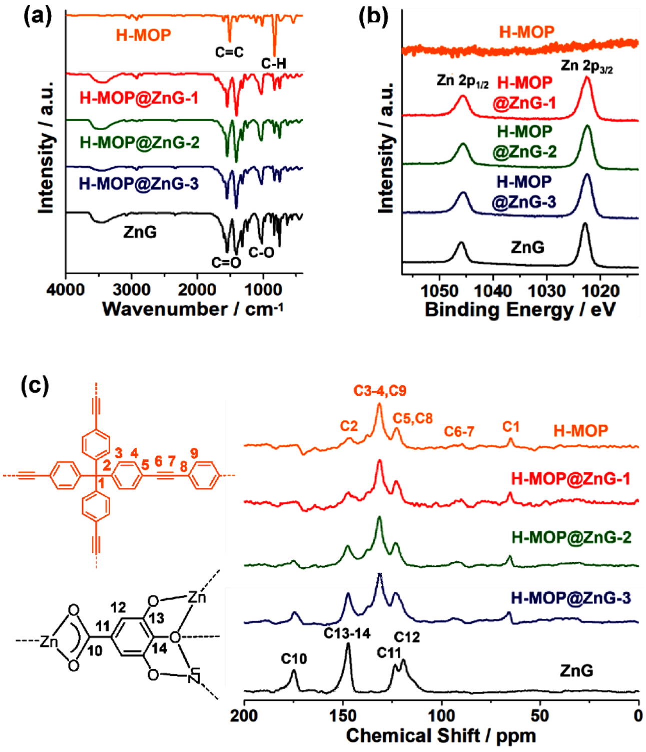

Figure 5. (a) IR absorption spectra, (b) XPS Zn $2p_{1/2}$ and $2p_{3/2}$ orbital spectra, and (c) solid-state CP/TOSS ^{13}C NMR spectra of H-MOP, H-MOP@ZnGs, and ZnG.

The IR spectrum of H-MOP showed main peaks at 1507 and 823 cm^{-1}, corresponding to aromatic C═C and C−H vibrations, respectively, matching with those of MOP materials reported in the literature (Figure 5a).[44] In comparison, the IR spectra of H-MOP@ZnGs showed main peaks at 1540, 1403, and 1026 cm^{-1}, corresponding to the C═O vibration of carboxylate groups and aromatic C═C and C−O vibrations of gallates, respectively, matching well with those of ZnG (Figure 5a). In the XPS spectra of H-MOP@ZnGs and ZnG, Zn $2p_{1/2}$ and $2p_{3/2}$ orbital peaks were clearly observed at 1045.7 and 1022.4 eV, respectively, indicating that the Zn species in the materials have an oxidation state of +2 (Figure 5b).[42] The solid-state ^{13}C NMR spectrum of H-MOP showed aromatic carbon peaks at 146.8, 137.6, 131.3, and 122.7 ppm, in addition to alkyne peaks at 87−95 ppm and a sp^3 carbon peak at 64.7 ppm (Figure 5c).[49] In comparison, the solid-state ^{13}C NMR spectrum of ZnG showed a carbonyl carbon peak of carboxylate groups at 174.9 ppm and aromatic carbon peaks at 147.3 (aromatic carbons adjacent to oxygens), 123.5, and 119.2 ppm.[42] As the amounts of ZnG in H-MOP@ZnGs increased, intensities of the corresponding ^{13}C peaks of ZnG gradually increased.

According to water contact angle (WCA) measurements, while ZnG was completely hydrophilic, H-MOP showed hydrophobicity with a WCA of 139° due to its organic nature. As expected, H-MOP@ZnG-2 with a WCA of 49° was hydrophilic (Figure S3).

Considering the uniformity of the ZnG coating toward H-MOP, we determined H-MOP@ZnG-2 as an optimal material.

Considering the active surface of ZnG for carbon dioxide conversion, we studied the performance of H-MOP@ZnG-2 as a heterogeneous catalyst for the reductive carbon dioxide fixation to formamides. Moreover, a morphology effect of H-MOP@ZnG-2 was studied and compared with ZnG. Table 1 and Figures 6−8 summarize the results.

Table 1. Reductive Carbon Dioxide Fixation to Formamides Catalyzed by H-MOP@ZnG-2[a]

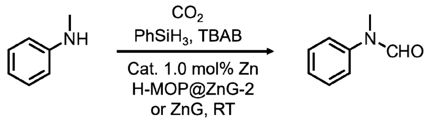

entry	$PhSiH_3$ (mmol)	TBAB (mol %)	CO_2 (bar)	time (h)	conv[b] (%)	yield[c] (%)
1[d]	2.0	1.0	10	1	1.2	0.8
2[d]	2.0	1.0	10	3	1.9	1.6
3[d]	2.0	1.0	10	6	11	10
4[d]	2.0	1.0	10	9	45	44
5[d]	2.0	1.0	10	12	46	46
6	2.0	1.0	10	1	13	11
7	2.0	1.0	10	3	41	39
8	2.0	1.0	10	6	77	74
9	2.0	1.0	10	9	93	91
10	2.0	1.0	10	12	99	97[e]
11[f]	2.0	1.0	10	12	3.6	3.1
12	2.0	0	10	12	0	0
13	1.0	1.0	10	12	41	40
14	0	1.0	10	12	0	0
15	2.0	1.0	5	12	35	32
16	2.0	1.0	1	12	0	0
17[g]	2.0	1.0	10	12	98	98
18[h]	2.0	1.0	10	12	99	98
19[i]	2.0	1.0	10	12	99	97
20[j]	2.0	1.0	10	12	99	97

[a] Reaction conditions: *N*-methyl-*N*-phenylamine (1.0 mmol), $PhSiH_3$ (0−2.0 mmol), tetrabutylammonium bromide (TBAB, 0−1.0 mol % to *N*-methyl-*N*-phenylamine), CO_2 (1−10 bar), H-MOP@ZnG-2 (1.0 mol % Zn to *N*-methyl-*N*-phenylamine), acetonitrile (3 mL), and 25 °C. [b] Conversion yields of *N*-methyl-*N*-phenylamine. [c] Yields of *N*-methyl-*N*-phenylformamide. [d] ZnG (1.0 mol % Zn to *N*-methyl-*N*-phenylamine) was used as a catalyst. [e] An isolated yield was also 97%. [f] No catalysts were used. [g] The catalyst recovered from entry 10 was used. [h] The catalyst recovered from entry 17 was used. [i] The catalyst recovered from entry 18 was used. [j] The catalyst recovered from entry 19 was used.

At first, we used *N*-methyl-*N*-phenylamine and 10 bar of carbon dioxide with 2 equiv of phenylsilane and a cocatalyst of 1.0 mol % tetrabutylammonium bromide (TBAB). Under this reaction condition, the ZnG with 1.0 mol % Zn showed gradual formation of *N*-methyl-*N*-phenylformamide with yields of 0.8, 1.6, 10, 44, and 46% after 1, 3, 6, 9, and 12 h at room temperature, respectively (entries 1−5 in Table 1 and Figure 6a). It is also noteworthy that ZnG required an induction time to show catalytic activity, indicating that aggregates of ZnG plates need to reorganize to show catalytic activity. In comparison, under the same reaction conditions, H-MOP@ZnG-2 with 1.0 mol % Zn showed fast and efficient formation of *N*-methyl-*N*-phenylformamide with yields of 11, 39, 74, 91, and 97% after 1, 3, 6, 9, and 12 h at room temperature, respectively (entries 6−10 in Table 1 and Figure 6a). These observations imply that engineering of ZnG on H-MOP platforms could enhance its catalytic activity due to facilitated contact of substrates with Zn species (Figure 6b).[43] It is also noteworthy that H-MOP@Zn-2 showed the enhanced CO_2

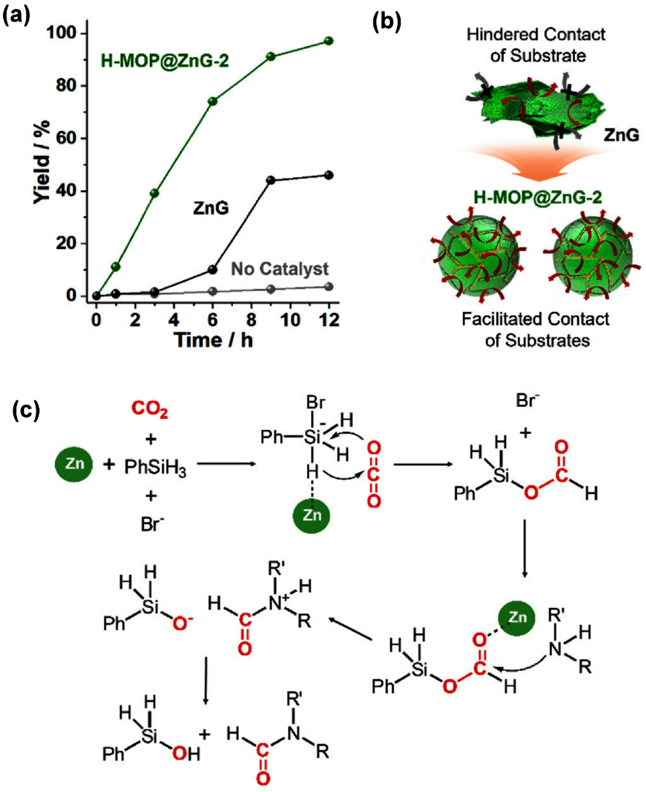

Figure 6. (a) Control tests of H-MOP@ZnG-2 (1.0 mol % Zn), ZnG (1.0 mol % Zn), and no catalyst systems for the reductive carbon dioxide fixation to *N*-methyl-*N*-phenylformamide (reaction conditions: 1.0 mmol of *N*-methyl-*N*-phenylamine, 2.0 mmol of $PhSiH_3$, 1.0 mol % TBAB, 10 bar of CO_2, 3 mL of acetonitrile, 25 °C). (b) Illustration of the morphology effect of H-MOP@ZnG-2 and ZnG. (c) Mechanism of carbon dioxide fixation to formamide with phenylsilane and amines catalyzed by H-MOP@ZnG-2.

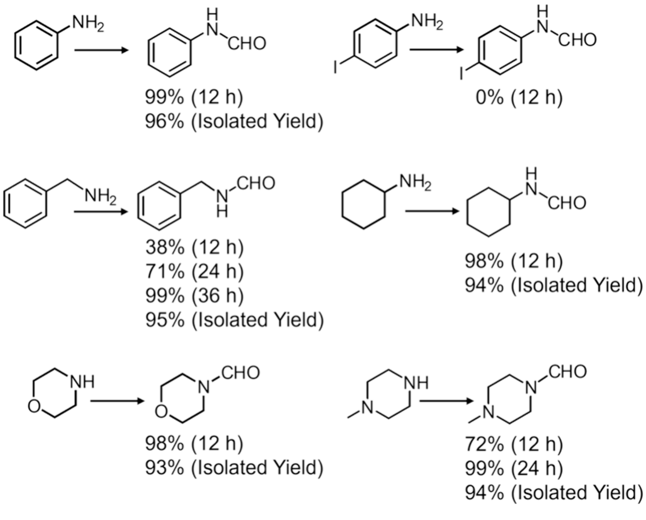

Figure 7. Amine substrate-dependent reductive carbon dioxide fixation to various formamides (reaction conditions: 1.0 mol % Zn in H-MOP@ZnG-2, 1.0 mmol of amines, 2.0 mmol of $PhSiH_3$, 1.0 mol % TBAB, 10 bar of CO_2, 3 mL of acetonitrile, 25 °C). Isolated yields were obtained by column chromatography.

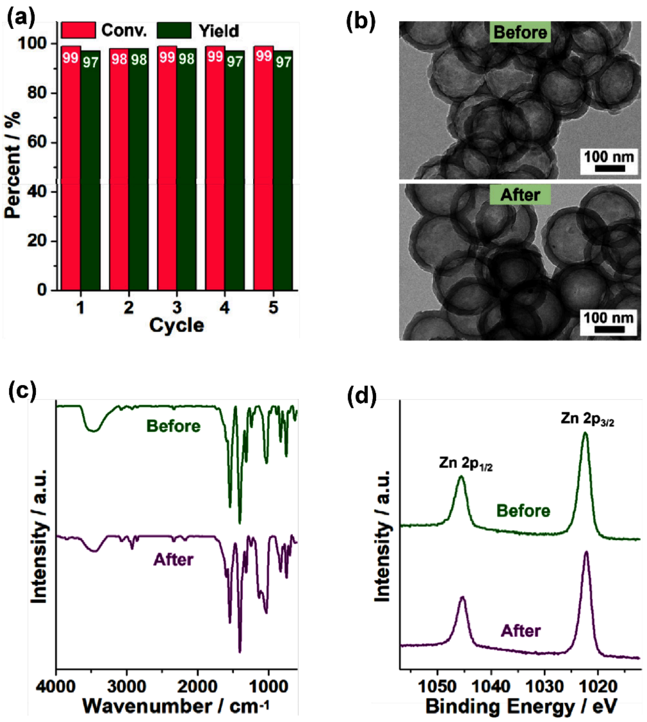

Figure 8. (a) Recyclability tests of H-MOP@ZnG-2 for the reductive carbon dioxide fixation to *N*-methyl-*N*-phenylformamide (reaction conditions: 1.0 mmol of *N*-methyl-*N*-phenylamine, 2.0 mmol of $PhSiH_3$, 1.0 mol % TBAB, 1.0 mol % Zn in H-MOP@ZnG-2, 10 bar of CO_2, 3 mL of acetonitrile, 12 h, 25 °C). (b) TEM images, (c) IR absorption spectra, and (d) XPS Zn $2p_{1/2}$ and $2p_{3/2}$ orbital spectra of H-MOP@ZnG-2 before and after five successive reactions.

uptake (1.19 and 0.74 mmol/g at 273 and 298 K, respectively) and heat of adsorption (Q_{st}) of 18−25 kJ/mol, compared with those of ZnG (0.22 and 0.17 mmol/g at 273 and 298 K, respectively, and Q_{st} of 4.5−9.3 kJ/mol) (Figure S4).

Without H-MOP@ZnG-2, only a 3.1% yield of *N*-methyl-*N*-phenylformamide was obtained (entry 11 in Table 1), indicating that the reductive carbon dioxide fixation to *N*-methyl-*N*-phenylformamide was catalyzed by H-MOP@ZnG-2. When no TBABs were used, reductive carbon dioxide fixation did not occur (entry 12 in Table 1). When amounts of phenylsilane gradually decreased from 2 equiv to 1 and 0 equiv, yields of *N*-methyl-*N*-phenylformamide decreased from 97% to 40 and 0%, respectively (entries 10, 13, and 14 in Table 1). When the pressures of carbon dioxide decreased from 10 bar to 5 and 1 bar, the yields of *N*-methyl-*N*-phenylformamide gradually decreased from 97% to 32 and 0%, respectively (entries 10, 15, and 16 in Table 1). Thus, we determined 1 equiv of amine, 2 equiv of phenylsilane, 1.0 mol % TBAB, 1.0 mol % Zn of H-MOP@ZnG-2, 10 bar of CO_2, and room temperature as optimal reaction conditions.

Control tests showed that phenylsilane, TBAB, and H-MOP@ZnG are all essential for the successful reductive carbon dioxide fixation to formamides (entries 10−12 and 14 in Table 1). Based on these results, we suggest a reaction mechanism, as displayed in Figure 6c.

First, bromide of TBAB induced the formation of pentavalent silicate salt through a reaction with phenylsilane.[11,21,50] Zinc species in H-MOP@ZnG-2 further activated the pentavalent silicate salt to induce the nucleophilic attack of hydride to carbon dioxide, forming phenylsilyl formate and generating bromide. Second, Zn species in H-MOP@ZnG-2 activated the carbonyl group of phenylsilyl formate to induce nucleophilic attack of the amine. Finally, through a proton shift, formamide and phenylsilanol were formed.

Next, various amines were tested as substrates for the reductive carbon dioxide fixation catalyzed by H-MOP@ZnG-2 to formamides (Figure 7). When aniline was used under optimized reaction conditions instead of *N*-methyl-*N*-phenylamine, the reaction was successful, showing a 99% yield of *N*-phenylformamide after 12 h. In comparison, when 4-iodoaniline was used as a substrate, no conversion to formamide was observed even after 12 h, indicating that proper nucleophilicity of amines was critical for successful carbon dioxide fixation to formamides. When benzylamine was used, *N*-benzylformamide was slowly formed with yields of 38, 71, and 99% after 12, 24, and 36 h, respectively. It is known that benzylamine has a lower nucleophilicity than aniline. Thus, benzylamine required a longer reaction time for carbon dioxide fixation to *N*-benzylformamide compared with that of aniline.

Cyclohexylamine and morpholine were good substrates, showing 98 and 98% yields of *N*-cyclohexylforamide and morpholine-4-carbaldehyde after 12 h, respectively. In the case of 4-methylpiperazine, 4-methylpiperazine-1-carbaldehyde was formed with yields of 72 and 99% after 12 and 24 h, respectively. These results indicate that relatively electron rich aromatic and aliphatic amines are beneficial for the reductive carbon dioxide fixation to formamides due to their proper nucleophilicity.

According to TGA, H-MOP@ZnG-2 was thermally stable up to 254 °C (Figure S5). Considering the mild reaction conditions (room temperature) and thermal stability of H-MOP@ZnG-2, a recyclability test of the catalyst was conducted for the reductive carbon dioxide fixation to *N*-methyl-*N*-phenylformamides (Figure 8). During five successive runs, yields of *N*-methyl-*N*-phenylformamide were retained in the range 97−98% (Figure 8a and entries 10 and 17−20 in Table 1). When H-MOP@ZnG-2 was removed through filtration, the reaction stopped (Figure S6). ICP-AES analysis of the reaction mixture revealed only 0.46% leaching of Zn, indicating the heterogeneous nature of the catalytic system. TEM analysis of H-MOP@ZnG-2 retrieved after five successive runs showed complete retention of the original hollow structure, indicating its mechanical stability, due to the cross-linked polymeric nature of hollow platforms (Figure 8b). The H-MOP@ZnG-2 retrieved after reactions maintained a high surface area of 407 m^2/g (Figure S7). IR and solid-state ^{13}C NMR studies on the recovered H-MOP@ZnG-2 showed retention of the main vibration peaks at 1540, 1403, and 1026 cm^{-1} and a carbonyl carbon peak of carboxylate groups at 174.9 ppm, indicating that the original chemical structure of ZnG in H-MOP@ZnG-2 was maintained (Figures 8c and S7). In addition, XPS analysis of the retrieved H-MOP@ZnG-2 showed the maintenance of the original Zn(II) state during the reactions (Figure 8d).

For the past decade, various Lewis acid catalysts have been developed for the reductive carbon dioxide fixation to formamides.[11−30,34−38] For example, homogeneous catalysts bearing Zn, Cu, and Fe have been reported with TONs of 30−198 and TOFs of 1−33 h^{-1} for the reductive carbon dioxide fixation with *N*-methyl-*N*-phenylamine to *N*-methyl-*N*-phenylformamide at temperatures of 25−60 °C (refer to Table S2 for recent homogeneous catalytic systems).[11−17]

Recently, new heterogeneous catalysts have been developed with TONs of 9−70 and TOFs of 1−3 h^{-1} for the reductive carbon dioxide fixation with *N*-methyl-*N*-phenylamine or aniline to *N*-methyl-*N*-phenylformamide or *N*-phenylformamide at temperatures of 25−130 °C (refer to Table S3 for the performance survey of recent heterogeneous catalytic systems).[18−30] Especially, Zn-based heterogeneous catalysts have shown TONs of 14−40 and TOFs 1−2 h^{-1} for the reductive carbon dioxide fixation with *N*-methyl-*N*-phenylamine to *N*-methyl-*N*-phenylformamide at temperatures of 60−120 °C (refer to Table S4 for recent Zn-based heterogeneous catalytic systems).[34−38] Thus, further exploration of more efficient heterogeneous catalytic systems is required. In this regard, the H-MOP@ZnG-2 showing a TON of 97 and a TOF of 8 h^{-1} at room temperature is quite promising. The excellent catalytic performance of H-MOP@ZnG-2 is attributable to its hollow structure-induced facile mass transfer of substrates due to the reduced diffusion pathway and the enhanced utilization of active Zn sites (Figure 6b).[43]

CONCLUSIONS

A new efficient heterogeneous catalyst was developed through ZnG loading on hollow MOP platforms for the reductive conversion of carbon dioxide with amines to formamides. After the amount optimization of ZnG, the H-MOP@ZnG-2 with a homogeneous loading of ZnG was engineered. Compared with ZnG, H-MOP@ZnG-2 showed a much enhanced catalytic performance for the reductive carbon dioxide fixation with amines to formamides at room temperature. Moreover, the catalytic performance of H-MOP@ZnG-2 was superior to those of Zn-based recent heterogeneous catalysts in the literature. The excellent catalytic performance of H-MOP@ZnG-2 was attributed to the hollow structure-induced facilitated contact of substrates with Lewis acidic Zn species and the efficient utilization of catalytic ZnG materials by generating more particles. We believe that H-MOP@ZnG-2 can be further applied for various carbon dioxide conversions to valuable chemicals.

ASSOCIATED CONTENT

Supporting Information

The Supporting Information is available free of charge at https://pubs.acs.org/doi/10.1021/acsanm.4c01287.

> TEM images of H-MOP, ^{1}H and ^{13}C NMR spectra of formamides, water contact angles, CO_2 uptake properties, a TGA curve, a filtration test of H-MOP@ZnG-2, solid-state ^{13}C NMR spectra and surface areas before and after reactions, catalytic performance survey tables of homogeneous and heterogeneous catalysts in the literature (PDF)

AUTHOR INFORMATION

Corresponding Author

Seung Uk Son − *Department of Chemistry, Sungkyunkwan University, Suwon 16419, Korea;* orcid.org/0000-0002-4779-9302; Email: sson@skku.edu

Authors

Hyun Su Kim − *Department of Chemistry, Sungkyunkwan University, Suwon 16419, Korea*

June Young Jang − *Department of Chemistry, Sungkyunkwan University, Suwon 16419, Korea*

Yoon-Joo Ko − *Laboratory of Nuclear Magnetic Resonance, NCIRF, Seoul National University, Seoul 08826, Korea*

Hye-Young Jang − *Department of Energy Systems Research, Ajou University, Suwon 16499, Korea;* orcid.org/0000-0003-4471-2328

Complete contact information is available at: https://pubs.acs.org/10.1021/acsanm.4c01287

Notes

The authors declare no competing financial interest.

ACKNOWLEDGMENTS

This work was supported by the Carbon to X Program (2020M3H7A1098283) and the National Research Foundation of Korea (NRF) grant (RS-2023-00208797) funded by the Ministry of Science and ICT, Republic of Korea.

REFERENCES

(1) Sanz-Pérez, E. S.; Murdock, C. R.; Didas, S. A.; Jones, C. W. Direct Capture of CO_2 from Ambient Air. *Chem. Rev.* **2016**, *116*, 11840−11876.

(2) Artz, J.; Muller, T. E.; Thenert, K.; Kleinekorte, J.; Meys, R.; Sternberg, A.; Bardow, A.; Leitner, W. Sustainable Conversion of Carbon Dioxide: An Integrated Review of Catalysis and Life Cycle Assessment. *Chem. Rev.* **2018**, *118*, 434−504.

(3) Liu, Q.; Wu, L.; Jackstell, R.; Beller, M. Using Carbon Dioxide as a Building Block in Organic Synthesis. *Nat. Commun.* **2015**, *6*, 5933.

(4) Rudolph, M. A.; Isbrücker, P.; Schomäcker, R. Bifunctional Catalysts for the Conversion of CO_2 into Value-Added Products - Distance as a Design Parameter for New Catalysts. *Catal. Sci. Technol.* **2023**, *13*, 3469−3482.

(5) Lidston, C. A. L.; Severson, S. M.; Abel, B. A.; Coates, G. W. Multifunctional Catalysts for Ring-Opening Copolymerizations. *ACS Catal.* **2022**, *12*, 11037−11070.

(6) Darensbourg, D. J. Making Plastics from Carbon Dioxide: Salen Metal Complexes as Catalysts for the Production of Polycarbonates from Epoxides and CO_2. *Chem. Rev.* **2007**, *107*, 2388−2410.

(7) Li, Z.; Yu, Z.; Luo, X.; Li, C.; Wu, H.; Zhao, W.; Li, H.; Yang, S. Recent Advances in Liquid Hydrosilane-Mediated Catalytic N-Formylation of Amines with CO_2. *RSC Adv.* **2020**, *10*, 33972−34005.

(8) Liu, X.-F.; Li, X.-Y.; He, L.-N. Transition Metal-Catalyzed Reductive Functionalization of CO_2. *Eur. J. Org. Chem.* **2019**, *2019*, 2437−3447.

(9) He, C.; Zou, Y.-H.; Si, D.-H.; Chen, Z.-A.; Liu, T.-F.; Cao, R.; Huang, Y.-B. A Porous Metal-Organic Cage Liquid for Sustainable CO_2 Conversion Reactions. *Nat. Commun.* **2023**, *14*, 3317.

(10) He, C.; Si, D.-H.; Huang, Y.-B.; Cao, R. A CO_2-Masked Carbene Functionalized Covalent Organic Framework for Highly Efficient Carbon Dioxide Conversion. *Angew. Chem., Int. Ed.* **2022**, *61*, No. e202207478.

(11) Luo, R.; Lin, X.; Chen, Y.; Zhang, W.; Zhou, X.; Ji, H. Cooperative Catalytic Activation of Si-H Bonds: CO_2-Based Synthesis of Formamides from Amines and Hydrosilanes under Mild Conditions. *ChemSusChem* **2017**, *10*, 1224−1232.

(12) Luo, R.; Lin, X.; Lu, J.; Zhou, X.; Ji, H. Zinc Phthalocyanine as an Efficient Catalyst for Halogen-Free Synthesis of Formamides from Amines via Carbon Dioxide Hydrosilylation under Mild Conditions. *Chin. J. Catal.* **2017**, *38*, 1382−1389.

(13) Li, X.-D.; Xia, S.-M.; Chen, K.-H.; Liu, X.-F.; Li, H.-R.; He, L.-N. Copper Catalysis: Ligand-Controlled Selective N-Methylation or N-Formylation of Amines with CO_2 and Phenylsilane. *Green Chem.* **2018**, *20*, 4853−4858.

(14) Li, W.-D.; Zhu, D.-Y.; Li, G.; Chen, J.; Xia, J. B. Iron-Catalyzed Selective N-Methylation and N-Formylation of Amines with CO_2. *Adv. Synth. Catal.* **2019**, *361*, 5098−5104.

(15) Takaishi, K.; Nath, B. D.; Yamada, Y.; Kosugi, H.; Ema, T. Unexpected Macrocyclic Multinuclear Zinc and Nickel Complexes that Function as Multitasking Catalysts for CO_2 Fixations. *Angew. Chem., Int. Ed.* **2019**, *58*, 9984−9988.

(16) Zhang, Q.; Lin, X.-T.; Fukaya, N.; Fujitani, T.; Sato, K.; Choi, J.-C. Selective N-Formylation/N-Methylation of Amines and N-Formylation of Amides and Carbamates with Carbon Dioxide and Hydrosilanes: Promotion of the Basic Counter Anions of the Zinc Catalyst. *Green. Chem.* **2020**, *22*, 8414−8422.

(17) Sahoo, S.; Manna, S.; Rit, A. N-Heterocyclic Carbene Supported Zinc Catalyzed N-Formylation of Diverse N-H Functionalities with Carbon Dioxide under Ambient Conditions. *Catal. Sci. Technol.* **2023**, *13*, 3344−3350.

(18) Cui, X.; Zhang, Y.; Deng, Y.; Shi, F. Amine Formylation via Carbon Dioxide Recycling Catalyzed by a Simple and Efficient Heterogeneous Palladium Catalyst. *Chem. Commun.* **2014**, *50*, 189−191.

(19) Mitsudome, T.; Urayama, T.; Fujita, S.; Maeno, Z.; Mizugaki, T.; Jitsukawa, K.; Kaneda, K. A Titanium Dioxide Supported Gold Nanoparticle Catalyst for the Selective N-Formylation of Functionalized Amines with Carbon Dioxide and Hydrogen. *ChemCatChem* **2017**, *9*, 3632−3636.

(20) Lv, H.; Wang, W.; Li, F. Porous Organic Polymers with Built-in N-Heterocyclic Carbenes: Selective and Efficient Heterogeneous Catalyst for the Reductive N-Formylation of Amines with CO_2. *Chem.—Eur. J.* **2018**, *24*, 16588−16594.

(21) Chen, Y.; Luo, R.; Bao, J.; Xu, Q.; Jiang, J.; Zhou, X.; Ji, H. Function-Oriented Ionic Polymers Having High-Density Active Sites for Sustainable Carbon Dioxide Conversion. *J. Mater. Chem. A* **2018**, *6*, 9172−9182.

(22) Shen, Q.; Chen, X.; Tan, Y.; Chen, J.; Chen, L.; Tan, S. Metal-Free N-Formylation of Amines with CO_2 and Hydrosilane by Nitrogen-Doped Graphene Nanosheets. *ACS Appl. Mater. Interfaces* **2019**, *11*, 38838−38848.

(23) Chowdhury, A. H.; Kayal, U.; Chowdhury, I. H.; Ghosh, S.; Islam, S. Nanoporous ZnO Supported CuBr (CuBr/ZnO): An Efficient Catalyst for CO_2 Fixation Reactions. *ChemistrySelect* **2019**, *4*, 1069−1077.

(24) Phatake, V. V.; Ahire, J. P.; Bhanage, B. M. L-Serine@ZnO as an Efficient and Reusable Catalyst for Synthesis of Cyclic Carbonates and Formamides in Presence of CO_2 Atmosphere. *Mol. Catal.* **2020**, *492*, 111000.

(25) Zhou, Z.; Liu, X.; Ma, J.-G.; Cheng, P. MOF-Incorporated Binuclear N-Heterocyclic Carbene-Cobalt Catalyst for Efficient Conversion of CO_2 to Formamides. *ChemSusChem* **2022**, *15*, No. e202201386.

(26) Zhai, G.; Liu, Q.; Ji, J.; Wu, Y.; Geng, J.; Hu, X. Recyclable Polymerized Lewis Acid Poly-BPh$(C_6F_5)_2$ Catalyzed Selective N-Formylation and N-methylation of Amines with Carbon Dioxide and Phenylsilanes. *J. CO_2 Util.* **2022**, *61*, 102052.

(27) Newar, R.; Kalita, R.; Akhtar, N.; Antil, N.; Chauhan, M.; Manna, K. N-Formylation of Amines Utilizing CO_2 by a Heterogeneous Metal-Organic Framework Supported Single-Site Cobalt Catalyst. *Catal. Sci. Technol.* **2022**, *12*, 6795−6804.

(28) Li, Z.; Li, H.; Yang, S. Carboxylate-Functionalized Zeolitic Imidazolate Framework Enables Catalytic N-Formylation Using Ambient CO_2. *Adv. Sustainable Syst.* **2022**, *6*, 2100380.

(29) Tang, X.-Y.; Liu, J.; Chen, P.-B.; Wu, C.-C.; Li, X.-J.; Pan, Y.-M.; Liang, Y. Effective N-Formylation of Amines with CO_2 in Anaerobic Fermentation Gas Catalyzed by Triply Synergistic Effect of Ionic Porous Organic Polymer. *ChemCatChem* **2023**, *15*, No. e202201351.

(30) Yoo, D. K.; Jhung, S. H. N-Formylation of Amines with CO_2 by Using Zr-Based Metal-Organic Frameworks: Contribution of Defect Sites of MOFs to N-Formylation. *Appl. Catal. A: Gen.* **2023**, *659*, 119170.

(31) Egorova, K.; Ananikov, V. P. Toxicity of Metal Compounds: Knowledge and Myths. *Organometallics* **2017**, *36*, 4071−4090.

(32) Darensbourg, D. J.; Holtcamp, M. W. Catalytic Activity of Zinc(II) Phenoxides Which Possess Readily Accessible Coordination Sites. Copolymerization and Terpolymerization of Epxodies and Carbon Dioxide. *Macromolecules* **1995**, *28*, 7577−7579.

(33) Darensbourg, D. J.; Holtcamp, M. W.; Struck, G. E.; Zimmer, M. S.; Niezgoda, S. A.; Rainey, P.; Robertson, J. B.; Draper, J. D.; Reibenspies, J. H. Catalytic Activity of a Series of Zn(II) Phenoxides for the Copolymerization of Epoxides and Carbon Dioxide. *J. Am. Chem. Soc.* **1999**, *121*, 107−116.

(34) Yang, Z.-Z.; Yu, B.; Zhang, H.; Zhao, Y.; Ji, G.; Liu, Z. Fluoro-Functionalized Polymeric N-Heterocyclic Carbene-Zinc Complexes: Efficient Catalyst for Formylation and Methylation of Amines with CO_2 as a C1-Building Block. *RSC Adv.* **2015**, *5*, 19613−19619.

(35) Khatun, R.; Biswas, S.; Islam, S.; Biswas, I. H.; Riyajuddin, S.; Ghosh, K.; Islam, S. M. Modified Graphene Oxide Based Zinc Composite: an Efficient Catalyst for N-Formylation and Carbamate Formation Reactions Through CO_2 Fixation. *ChemCatChem* **2019**, *11*, 1303−1312.

(36) Du, C.; Chen, Y. Zinc Powder Catalyzed Formylation and Urealation of Amines Using CO_2 as a C1 Building Block. *Chin. J. Chem.* **2020**, *38*, 1057−1064.

(37) Sarkar, P.; Chowdhury, A. H.; Riyajuddin, S.; Biswas, S.; Ghosh, K.; Islam, S. M. Zn(II)@TFP-DAQ COF: An Efficient Mesoporous Catalyst for the Synthesis of N-methylated Amine and Carbamate Through Chemical Fixation of CO_2. *New J. Chem.* **2020**, *44*, 744−752.

(38) Lin, X.-T.; Matsumoto, K.; Maegawa, Y.; Takeuchi, K.; Fukaya, N.; Sato, K.; Inagaki, S.; Choi, J.-C. Immobilized $Zn(OAc)_2$ on Bipyridine-Based Periodic Mesoporous Organosilica for N-formylation of Amines with CO_2 and Hydrosilanes. *New J. Chem.* **2021**, *45*, 9501−8505.

(39) Soga, K.; Imai, E.; Hattori, I. Alternating Copolymerization of CO_2 and Propylene Oxide with the Catalysts Prepared from $Zn(OH)_2$ and Various Dicarboxylic Acids. *Polym. J.* **1981**, *13*, 407−140.

(40) Ree, M.; Hwang, Y.; Kim, J.-S.; Kim, H.; Kim, G.; Kim, H. New Findings in the Catalytic Activity of Zinc Glutarate and Its Application in the Chemical Fixation of CO_2 into Polycarbonates and Their Derivatives. *Catal. Today* **2006**, *115*, 134−145.

(41) Klaus, S.; Lehenmeier, M.; Herdtweck, E.; Deglmann, P.; Ott, A. K.; Rieger, B. Mechanistic Insights into Heterogeneous Zinc Dicarboxylates and Theoretical Considerations for CO_2-Epoxide Copolymerization. *J. Am. Chem. Soc.* **2011**, *133*, 13151−13161.

(42) Yang, Y.; Sung, K.; Lee, J. D.; Ha, J.; Kim, H.; Baek, J.; Seo, J. H.; Kim, S.-J.; Lee, B. Y.; Son, S. U.; Kim, B.-S.; Kim, Y.; Park, J.-Y.; Jang, H.-Y. Ultra-Thin Zn-Gallate Catalyst: A Remarkable Performer in CO_2 and Propylene Oxide Polymerization. *ACS Sustainable Chem. Eng.* **2024**, *12*, 3933.

(43) Prieto, G.; Tüysüz, H.; Duyckaerts, N.; Knossalla, J.; Wang, G.-H.; Schüth, F. Hollow Nano- and Microstructures as Catalysts. *Chem. Rev.* **2016**, *116*, 14056−14119.

(44) Lee, J. -S. M.; Cooper, A. I. Advances in Conjugated Microporous Polymers. *Chem. Rev.* **2020**, *120*, 2171−2214.

(45) Cho, K.; Kang, C. W.; Ryu, S. H.; Jang, J. Y.; Son, S. U. The Rise of Morphology-Engineered Microporous Organic Polymers (ME-MOPs): Synthesis and Benefits. *J. Mater. Chem. A* **2022**, *10*, 6950−6964.

(46) Stöber, W.; Fink, A.; Bohn, E. Controlled Growth of Monodisperse Silica Spheres in the Micron Size Range. *J. Colloid Interface Sci.* **1968**, *26*, 62−69.

(47) Ke, Z.; Zhang, Y.; Cui, X.; Shi, F. Supported Nano-gold-catalyzed N-formylation of Amines with Paraformaldehyde in Water Under Ambient Conditions. *Green Chem.* **2016**, *18*, 808−816.

(48) Nguyen, T. V. Q.; Yoo, W.-J.; Kobayashi, S. Effective Formylation of Amines with Carbon Dioxide and Diphenylsilane Catalyzed by Chelating bis(tzNHC) Rhodium Complexes. *Angew. Chem., Int. Ed.* **2015**, *54*, 9209−9212.

(49) Kang, N.; Park, J. H.; Jin, M.; Park, N.; Lee, S. M.; Kim, H. J.; Kim, J. M.; Son, S. U. Microporous Organic Network Hollow Spheres: Useful Templates for Nanoparticulate Co_3O_4 Hollow Oxidation Catalysts. *J. Am. Chem. Soc.* **2013**, *135*, 19115−19118.

(50) Hulla, M.; Bobbink, F. D.; Das, S.; Dyson, P. J. Carbon Dioxide Based N-Formylation of Amines Catalyzed by Fluoride and Hydroxide Anions. *ChemCatChem* **2016**, *8*, 3338−3342.